JOURNAL OF SPACECRAFT AND ROCKETS
Vol. 41, No. 3, May–June 2004

Closed-Loop Missile Yaw Control via Manipulation of Forebody Flow Asymmetries

Mehul P. Patel*
Orbital Research Inc., Cleveland, Ohio 44143
Carl P. Tilmann†
U.S. Air Force Research Laboratory, Wright–Patterson Air Force Base, Ohio 45433
and
T. Terry Ng‡
University of Toledo, Toledo, Ohio 43606

A high-alpha, closed-loop flow-control system for missile yaw stabilization and enhanced maneuverability was designed, developed, and successfully demonstrated in a series of open- and closed-loop experiments on a fin-less 3:1 caliber tangent ogive missile model. The active flow-control-based yaw control system consisted of eight fast-response pressure sensors and eight deployable flow effectors arranged in concentric rings on the missile nose cone. The devices were integrated with a closed-loop controller that modulated the effectors to manipulate flow asymmetry around the missile forebody. Side forces caused by crossflow separation and forebody flow asymmetries were observed on the missile model between 40 and 60 deg alpha. Parametric studies showed that actuating flow effectors in certain configurations resulted in cancellation of large side forces associated with the natural flow asymmetry under both steady and unsteady flow conditions. Exploratory studies conducted on optimized flow effector configurations resulted in control maps with wide spectrum of positive and negative side forces for yaw modulation. Dynamic experiments successfully demonstrated the ability of the closed-loop control system to generate and maintain a range of desired yawing moments during high-alpha pitch sweeps.

Nomenclature

C_n = yawing-moment coefficient
C_Y = side-force coefficient
K_d = derivative gain of the control law
K_i = integral gain of the control law
K_p = proportional gain of the control law
Re_d = freestream Reynolds number
α = angle of attack, deg
β = angle of sideslip, deg
θ = flow effector circumferential orientation, deg

Introduction

IT has long been recognized that, at high alpha, slender bodies of revolution encounter separation- and vortex-induced yaw caused by asymmetric vortex shedding, even at zero angle of sideslip.[1–4] Large side forces and dynamic out-of-plane loadings occur for alpha ranging from 30 to 60 deg. Researchers have concluded that the out-of-plane loads result from microasymmetries on the surface of the nose cone such as small dents, cracks in the paint, and other imperfections near the tip of the nose cone.[5,6] It has also been shown that these asymmetries can be affected by the bluntness of the forebody, Reynolds number, roll angle, and alpha. These side forces are of great concern at high alpha because of the increasing ineffectiveness of traditional control surfaces. Side forces resulting from these asymmetries, also referred to as "phantom yaw" in some research circles, adversely affect the overall performance of missiles and fighter aircraft and significantly limit their flight envelope. The term phantom does not refer to the relatively well-understood fluid mechanics behind the phenomenon; rather, it refers to the general unpredictability and uncontrollability of conditions such as small nose cone imperfections and transient flow disturbances that dictate the magnitude and direction of the unintended yawing moment. Proper exploitation of this phenomenon by controlling the system of vortices along the forebody cannot only offset natural side forces but also produce desired side forces so as to significantly enhance missile stability and maneuverability at high alpha.

Next-generation high-performance missiles and fighter aircraft face a much greater challenge where mission requirements dictate evasive high-alpha maneuvers.[7] Demand for high-alpha missile control systems has led to a number of investigations on the subject.[8–12] Research conducted by Herbst, later followed by Ericsson and Beyers, demonstrated the ability to achieve supermaneuverability on a X-31 aircraft for extreme aerial combat situations using thrust vectoring and advanced control schemes such as movable forward canards and thrust vectoring.[13,14] Other investigators have used various forms of geometric changes such as nose bluntness, strakes, boundary-layer strips, and rotating nose tips to control the asymmetric vortices off the forebody.[15–19] A single symmetric strake and a splitter-plate-fin were also used to suppress the flow asymmetry.[20,21] It was shown that the splitter-plate-fin did not have to extend far downstream of the apex for controlling the asymmetric loads. Controlled disturbances at the near-apex flow region were able to control the flow downstream as a result of strong three-dimensional flow effects. Blowing has also been used to control forebody flow asymmetry.[22] Recent accomplishments using microblowing have demonstrated that vortex instabilities can be manipulated with small, controlled perturbations introduced near the region of maximum flow sensitivity, that is, the nose of the missile forebody.[23]

Passive flow-control techniques such as transition strips, vane vortex generators, and nose bluntness are fairly effective in alleviating aerodynamic loads, but are limited by increased parasitic drag and loss of vortex-induced lift on the forebody. This presents a need for active flow-control systems that not only mitigate flow asymmetry but also provide active force modulation to attain desired levels

Received 20 September 2002; revision received 30 April 2003; accepted for publication 3 July 2003.

*Director, Aerodynamics Group. Member AIAA.
†Senior Research Engineer, Air Vehicles Directorate. Senior Member AIAA.
‡Professor, Department of Mechanical, Industrial, and Manufacturing Engineering. Senior Member AIAA

of maneuverability. The system should also be able to deactivate control actuators when not required in order to minimize parasitic drag.

Researchers have investigated various active flow-control techniques such as jet blowing, unsteady bleed, suction and blowing, and flow effectors.[24–27] These techniques typically operate in an open-loop mode with no sensor feedback. Consequently, a robust closed-loop control system is a logical extension to such control systems in order to fully realize the potential of flow-control actuators for missile-control enhancement. Recently, researchers have investigated the feasibility of closed-loop control systems for high-alpha maneuvering via numerical and experimental investigations.[28–30] Bernhardt and Williams demonstrated the ability of a closed-loop control system to control the coning angle of the model, its rotation rate, and the direction of rotation, using a pair of suction ports on either side of the nosecone tip.[29] The input and the output command in the closed-loop control system used by Bernhardt and Williams was the pressure coefficient.[29] We conjecture that a closed-loop control system, which utilizes yawing moment rather than the pressure coefficient as the command parameter to the control system, can potentially improve controllability by reducing errors that typically arise from the indirect pressure-moment correlation. It is evident that a more accurate quantification of the phantom yaw on a missile body is the side force and not the pressure coefficient measured by a localized pressure sensor because the latter does not quantify the side forces arising from the missile body aft of the sensor location. Nevertheless, as dictated by the requirements of controlling unsteady flow dynamics, where fast sensor response in the vicinity of maximum flow sensitivity is required, fast-response pressure sensors are indispensable to the control system. In support of this argument, it is proposed that a combination of fast-response pressure sensors and a force sensor offer better understanding of system dynamics and hence improved controllability of side forces.

Nonetheless, despite numerous investigations, a robust closed-loop control system that fully realizes the potential of flow-control techniques for enhanced missile maneuverability at high alpha has yet to be identified. This paper presents a novel active flow-control system for missile yaw control at high alpha, using pressure sensors, a force balance, forebody deployable actuators, and a closed-loop controller.

High-Alpha Yaw-Control System

The high-alpha yaw-control system utilized circumferential arrays of eight deployable flow effectors (DFEs) and eight fast-response (~500 Hz) pressure sensors, integrated with a force balance and a closed-loop controller. Figure 1 illustrates the principle of operation of the DFE-based yaw-control system. During this study, pressure sensors captured instantaneous pressure distribution around the missile forebody, while a force balance measured side forces resulting from the asymmetric pressure distribution. Correlation between the pressure data and the force balance data at specific flowfield events was used to develop an effective feedback control parameter for the controller. The side-force coefficient C_Y was used as the control parameter for static tests; however, because of the dynamic nature of the flow during pitching maneuvers, instantaneous pressure signal from fast-response pressure sensors was used as the control parameter for dynamic tests. Based on the error between the measured flow state and the desired flow state, the controller actively changed the DFE deployment configuration so as to minimize the error. DFEs are active microvortex generators that manipulate the pressure distribution along the forebody, yielding large side forces for missile yaw control. Parameters used for optimizing the DFE deployment configuration for different alpha and flow conditions were 1) DFE circumferential location, 2) total number and specific combination of DFEs, and 3) frequency and duty cycle of each DFE. The control system relied upon the effectiveness of DFEs in controlling flow asymmetries to produce desired yawing moments on the missile body. Upon controlled deployment, the DFEs demonstrated the ability to control the baseline asymmetry as well as produce and maintain desired yawing moments on the model, during both steady and dynamic missile maneuvers. To obtain a wide and well-resolved spectrum of generated side forces, many DFE configurations were designed and investigated through static wind-tunnel tests. Details on the controller architecture for the closed-loop control system are as follows.

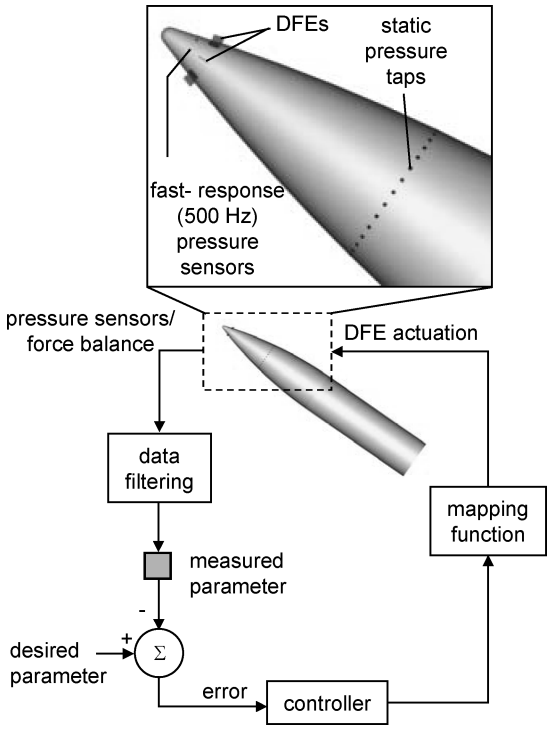

Fig. 1 Schematic of the DFE-based high-alpha yaw-control system.

Closed-Loop Control System

A digital closed-loop control system for high-alpha forebody vortex control was developed using a frequency-based proportional-integral-derivative (PID) control law. The optimum PID parameters based on an iterative procedure were found to be $K_p = 1.0$, $K_i = 0.3$, and $K_d = 0.2$. The block diagram for the feedback controller is shown in Fig. 2. The command input variable C_n representative of the desired yawing moment (left, right, or zero) was compared to the measured flow state C_n to obtain an error signal every 80 ms. The controller used a mapping function $f_n(x)$ to map the DFE deployment configuration with a time step of 5 ms for a period of 80 ms (controller time step) to null out the error. Based on the results from DFE optimization tests, two DFEs positioned at the most effective circumferential locations for creating opposing side forces on the missile body (positive and negative yaw) were chosen for closed-loop control experiments. A mapping function $f_n(x)$ specific to each DFE contained information about its deployment configuration and actuation time step for the duration of the controller time step. The parameters of the DFE deployment configuration used for the closed-loop control tests were frequency and the duty cycle. The limitation of DFE actuation time step was set to 5 ms to accommodate pneumatic lag associated with deploying the DFEs; however, the time step was sufficient for the control fidelity required for the closed-loop control study.

Missile Model and Experimental Facility

The model, as shown in Fig. 3, had a typical finless air-to-air missile geometry with a fineness ratio of 6.12 based on the maximum body diameter of 10.16 cm and 3:1 tangent ogive nose cone. The length and the tip radius of the missile model were 62.23 and 0.635 cm, respectively. The forebody contained circumferential arrays of eight DFEs and eight dynamic pressure sensors embedded at a distance of 3.2 and 4.1 cm, respectively, from the tip of the missile nose cone, as highlighted in Fig. 3. DFEs utilized in this study were made from epoxy glass-fabric board in the form of small mechanical

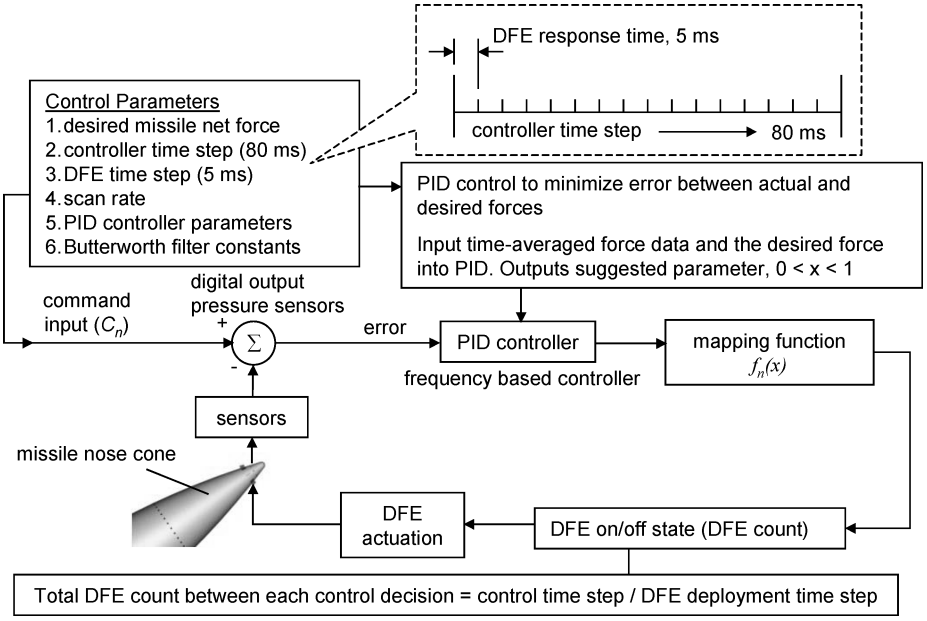

Fig. 2 Block diagram of the closed-loop flow-control system.

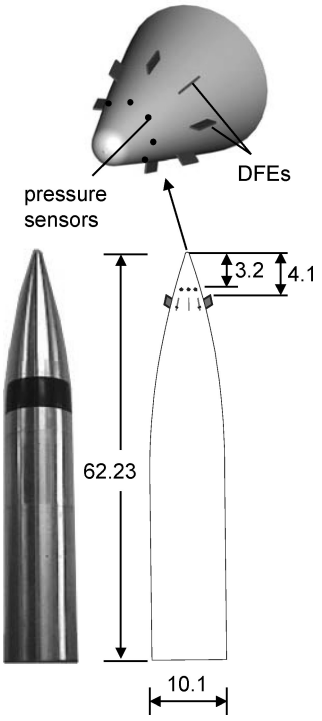

Fig. 3 Illustration of the missile model with a 3:1 tangent ogive nose. Units in centimeters.

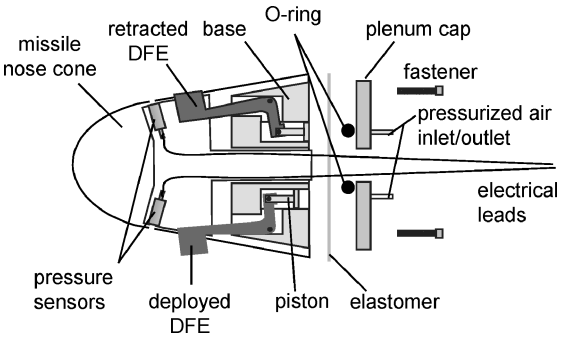

Fig. 4 Illustration of the missile nose cone with DFE actuation system.

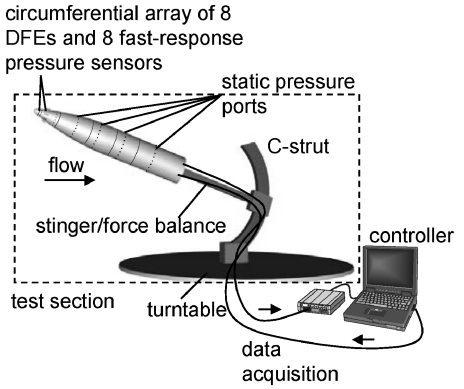

Fig. 5 Experimental setup for wind-tunnel testing.

tabs of length $l = 9$ mm, width $w = 0.8$ mm, and height $h = 3$ mm. They were flush mounted on the missile nose cone, nonobtrusive to the flow, and were deployed 1 mm outside the boundary layer when actuated. The forebody model contained a pneumatic control actuation system (Fig. 4) for flush mounting the DFEs (in the retracted state) on the missile nose cone, while allowing them to be deployed as required. In addition to the dynamic pressure sensors, the model was equipped with a total of 128 pressure taps (4 rings of 32 taps) to measure surface pressures at regular intervals along the missile body. The model was equipped with a sting-mounted, five-component (no axial force) force balance. Because of the round cross section of the model, no rolling moment could be generated, and the component was not recorded. Additionally, information on the flowfield around the missile body was gathered at several model locations using smoke and laser-sheet flow-visualization techniques. Figure 5 shows the experimental setup for wind-tunnel testing.

Wind-tunnel tests were performed at the University of Toledo Fluid Dynamics Laboratory in a 0.9×0.9 m closed-loop, low-speed wind tunnel. The model support incorporated a C-strut and a turntable for different α and β settings (Fig. 5). A positioning turntable was installed to facilitate dynamic tests on the model for α-sweep rates from 1 up to 35 deg/s. The positioning table was incorporated with an optical encoder feedback that offered accuracy up to 1 arcsec, axis wobble of less than 2 arcsec, and a repeatability of 0.2 arcsec. The flow in the test section was uniform with a turbulence level of 0.2% outside of wall boundary layers.

Wind-Tunnel Experiments

Open-loop experiments consisted of a series of static tests to characterize and optimize the effectiveness of DFEs in controlling forebody flow asymmetry at different α conditions. Closed-loop experiments included dynamic tests to evaluate the performance of the control law in actively updating the optimal DFE deployment configuration in order to achieve and hold a desired yaw moment during dynamic pitching maneuvers.

DFE Optimization Tests

Static wind-tunnel tests were performed for α ranging from 25 to 65 deg at a Re_d of 0.13×10^6 based on the freestream velocity of 20 m/s and model diameter of 10.16 cm. Specific objectives of the static tests were 1) to obtain an effective α range for the DFEs, 2) to identify optimal DFE circumferential locations, and 3) to generate control maps that define DFE saturation limits for the effective α range. To achieve these objectives, a first series of static tests as listed in Table 1 were performed for α ranging from 20 to 65 deg in increments of 5 deg at zero sideslip angle β. After identifying the effective α range, that is, 40 deg $< \alpha <$ 60 deg, tests were conducted at $\alpha = 40$, 45, and 55 deg to determine the optimal DFE circumferential location on the missile nose cone (Fig. 6). Table 2 lists the test matrix for the DFE optimization tests. The performance of DFE 1 was tested at varying circumferential position θ by rotating missile forebody from $\theta = 0$ to 40 deg in increments of 5 deg, where $\theta = 0$ corresponds to forward stagnation point $+\pi/2$. It was observed that the baseline (no DFE deployed) flow asymmetry on the symmetrical missile model varied nonuniformly upon forebody rotation. This observation necessitated further tests so as to broadly characterize the influence of missile forebody at different θ positions on flow asymmetry, that is, phantom yaw. Finally, in order to generate control maps with wide spectrum of positive and negative side forces for side-force modulation using DFEs static tests were conducted using a variety of DFE configurations for $\alpha = 40$, 45, and 50 deg at $\beta = 0$ deg (see Table 3). The selection of DFE deployment configurations, listed in Table 3, was based on the qualitative and quantitative observations made during the static experiments, which are discussed in the Results section of this paper.

Table 1 Test matrix to determine the effective alpha range for the DFEs

pitch α, deg	Sideslip β, deg	Actuated DFE no.							
20	0	0	1	2	3	4	5	6	7
25	0	0	1	2	3	4	5	6	7
30	0	0	1	2	3	4	5	6	7
35	0	0	1	2	3	4	5	6	7
40	0	0	1	2	3	4	5	6	7
45	0	0	1	2	3	4	5	6	7
50	0	0	1	2	3	4	5	6	7
55	0	0	1	2	3	4	5	6	7
60	0	0	1	2	3	4	5	6	7

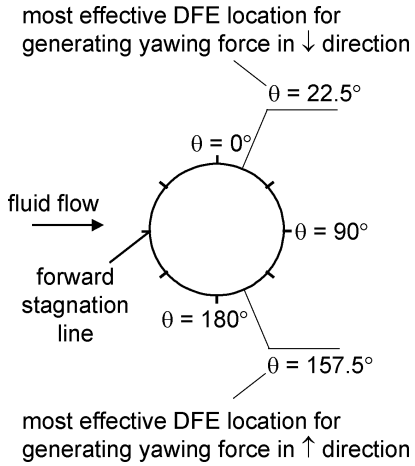

Fig. 6 Diagram showing DFE circumferential locations on the missile nose cone.

Table 2 Test matrix to determine optimal DFEs radial location on the missile nose cone

$\alpha = 40$ deg, $\beta = 0$ deg		$\alpha = 45$ deg, $\beta = 0$ deg		$\alpha = 50$ deg, $\beta = 0$ deg	
DFE no.	θ, deg	DFE no.	θ, deg	DFE no.	θ, deg
1	0	1	0	1	0
1	5	1	5	1	5
1	10	1	10	1	10
1	15	1	15	1	15
1	20	1	20	1	20
1	22.5	1	22.5	1	22.5
1	25	1	25	1	25
1	30	1	30	1	30
1	35	1	35	1	35
1	40	1	40	1	40
2	22.5	2	22.5	2	22.5
3	22.5	3	22.5	3	22.5
4	22.5	4	22.5	4	22.5
5	22.5	5	22.5	5	22.5
6	22.5	6	22.5	6	22.5
7	22.5	7	22.5	7	22.5
0	22.5	0	22.5	0	22.5

α-Sweep Tests

Dynamic-pitching tests were conducted at a Re_d of 0.13×10^6 for α sweeps from 0 to 60 deg at sweep rates of 10 and 35 deg/s. The main objective of the dynamic tests was to demonstrate the ability of the closed-loop control system in stabilizing and controlling forebody flow asymmetry at high-alpha flow conditions. First, the effect of dynamic α sweeps for pitching-up and pitching-down motions on the natural flow asymmetry of the missile model was characterized. Second, the effect of DFEs in controlling flow asymmetry to achieve positive and negative yawing moments was quantified. This was followed by control modulation tests, where the closed-loop control system was used in generating on-demand yawing moments for commanded values at $\alpha = 60$ deg and $\beta = 0$ deg. Finally, closed-loop dynamic-pitching tests at $\beta = 0$ deg were conducted where the control system's performance was evaluated in mitigating natural flow asymmetry as well as maintaining zero yaw during α sweep from 0 to 60 deg at 30- and 60-deg/s pitch rates.

Results and Discussion

Results from static wind-tunnel experiments are presented primarily in the form of control maps of side-force coefficient C_Y obtained via a series of DFE optimization tests, as tabulated in Tables 1–3. Accuracy of results was verified by repeated measurements, for both static and dynamic tests, that showed good repeatability. The first series of static tests (Table 1) revealed significant flow asymmetry from $\alpha = 35$ to 60 deg. This α range was predominantly influenced by forebody flow asymmetry, consistent with the observations made in the past by other researchers.[31,32] Flow conditions near the missile forebody for this α range were favorable for DFEs because of the presence of flow asymmetry in regions of maximum flow sensitivity.

For 40 deg $< \alpha <$ 60 deg DFEs were found to be effective in generating side forces large enough to offset baseline asymmetry as well as enhance and reverse flow asymmetry. Snapshots of laser-sheet flow visualization, shown in Fig. 7, demonstrate vortex reversal at 60 deg α using DFEs located at $\theta = 22.5$ and 157.5 deg. For $\alpha > 60$ deg no significant natural yawing moment (phantom yaw) was observed on the model because of the diminishing influence of forebody flow asymmetry.

Tests performed according to the matrix in Table 2 determined the optimized DFE circumferential location for $\alpha = 40$, 45, and 55 deg at $\beta = 0$ deg. Figure 8 shows a control map of side forces attainable by DFEs at $\alpha = 40$ deg and $\beta = 0$ deg. Tests revealed

Table 3 DFE configuration test matrix to obtain a wide spectrum of generated forces for $\alpha = 40$, 45, and 50 deg

No.	DFE no.	Deployment	Frequency, Hz	No.	DFE no.	Deployment	Frequency, Hz
1	5	Static	——	31	3, 5	——	6, 6
2	6	Static	——	32	3, 5	——	5, 3
3	5	——	6	33	3, 5	——	2, 7
4	5	——	8	34	3, 5	——	2, 4
5	5	——	14	35	3, 5	——	15, 10
6	5	——	20	36	3, 5	——	8, 12
7	5	——	11	37	3, 5	——	20, 14
8	5	——	17	38	3, 5	——	18, 13
9	5	——	3	39	3, 5	——	9, 6
10	5	——	1	40	3, 5	——	16, 8
11	5	——	5	41	3, 5	——	4, 1
12	5	——	2	42	3, 5	——	19, 7
13	5	——	4	43	3, 5	——	12, 16
14	5	——	1	44	3, 5	——	14, 20
15	5	——	3	45	3, 5	——	13, 3
16	5	——	1	46	3, 5	——	17, 11
17	5	——	2	47	3, 5	——	2, 3
18	0	Static	——	48	1	Static	——
19	6, 7	——	3, 2	49	3	——	14
20	5, 7	——	2, 1	50	3	——	20
21	5, 7	——	1, 2	51	3	——	17
22	6	——	5	52	3	——	4
23	6	——	4	53	3	——	2
24	4	Static	——	54	3	——	8
25	7	Static	——	55	3	——	5
26	3, 5	——	10, 5	56	3	——	11
27	3, 5	——	11, 4	57	2	Static	——
28	3, 5	——	7, 2	58	3	——	6
29	3, 5	——	3, 5	59	3	——	3
30	3, 5	——	3, 6	60	3	Static	——

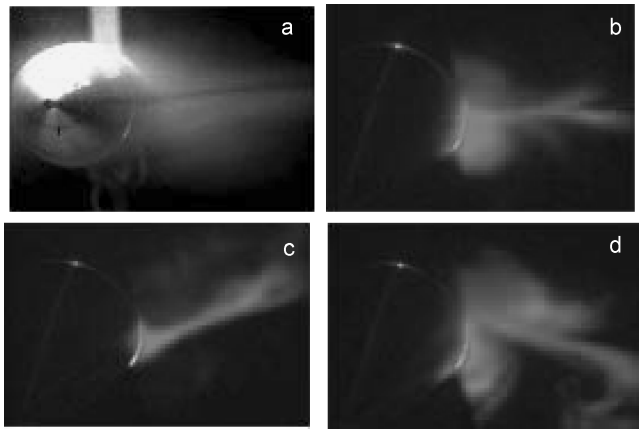

Fig. 7 Laser-sheet flow visualization on missile forebody at 60 deg α a) missile model orientation, b) baseline flow with no DFE, c) DFE actuated at 22.5 deg θ, and d) DFE actuated at 157.5 deg θ.

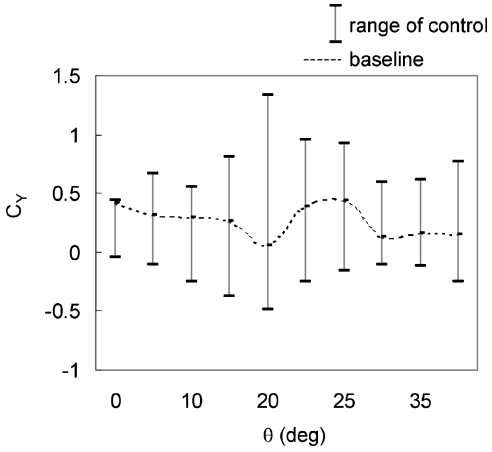

Fig. 8 Control map of attainable positive and negative side forces using DFE 1 at varying θ locations for 40 deg α and 0 deg β.

that the DFEs were most effective when deployed at the circumferential location between $\theta = 15$ and 25 deg, as shown in Fig. 8. The dashed curve cutting through the range-of-control vertical bars represents the baseline flow asymmetry at the corresponding DFE circumferential configuration. The range-of-control bars for DFE 1 at various θ locations were obtained by tests conducted according to the matrix in Table 3. Although the largest control forces were generated at $\theta = 22.5$ deg, the DFEs were able to generate forces large enough to cancel the baseline asymmetry for all cases. In most cases DFEs were able to reverse the baseline flow asymmetry with an equal magnitude or higher.

It was found that the statically deployed DFEs produced the largest side forces and the control effectiveness progressively diminished with increasing oscillation frequencies. Initial speculation, which was later confirmed by repeated experiments, led to proving that the timescales associated with the development and propagation of the vortices created by the DFEs was the key parameter in obtaining the desired level of side force on the missile body. It is hypothesized that a full static deployment of the DFE causes the maximum forebody vortex asymmetry to develop, whereas actuating the DFE at a given frequency results in short, pulsating disturbances, coupled with the time lag of vortex flow response, leading to suspension of forebody vortices in an immediate asymmetric state even at near bistable natural states. This theory formed the basis of selecting the different DFE deployment configurations as listed in Table 3.

DFE characterization tests conducted according to the matrix in Table 3 at $\alpha = 40$ deg and $\beta = 0$ deg provided a spectrum of side forces, shown in Fig. 9, encompassing both negative and positive yaw states using different DFE configurations, which comprised statically deployed DFEs and a combination of two or more DFEs operating at different oscillatory frequencies. This spectrum of side forces is translated into a vertical bar representing total range of control as shown in Fig. 8. Once the optimal circumferential location for DFE actuation, that is, $\theta = 22.5$ deg was determined, tests were conducted to obtain control maps of side forces using different DFEs

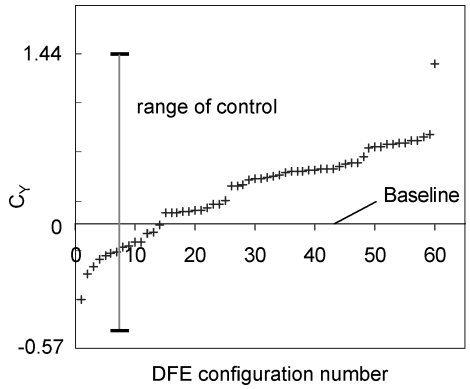

Fig. 9 Spectrum of side forces generated using different DFE configurations at 40 deg α and 0 deg β.

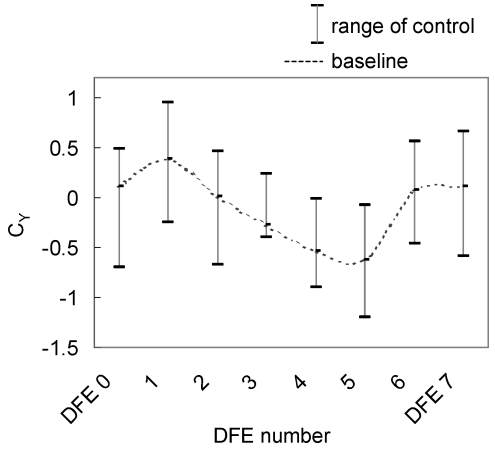

Fig. 10 Control map of side forces generated at 40 deg α and 0 deg β using different DFEs at 22.5 deg θ.

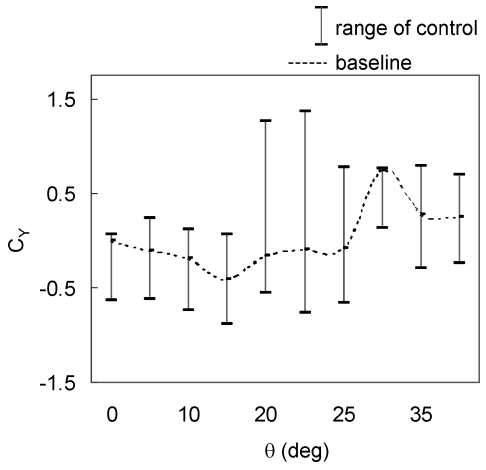

Fig. 11 Control map of attainable positive and negative side forces using DFE 1 at various θ locations for 45 deg α and 0 deg β.

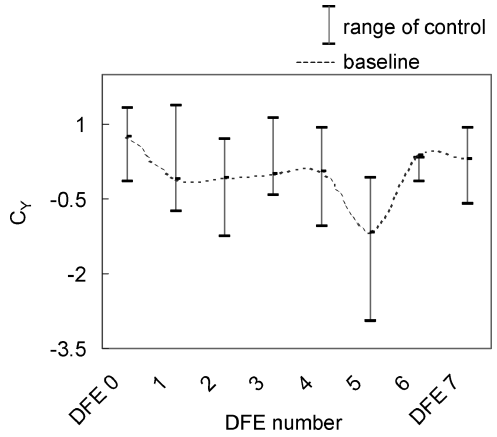

Fig. 12 Control map of side forces generated at 45 deg α and 0 deg β using different DFEs at 22.5 deg θ.

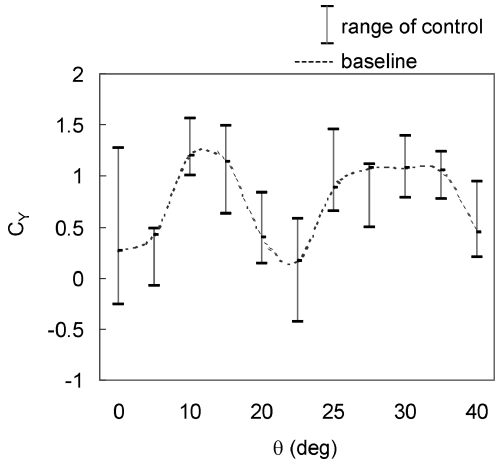

Fig. 13 Control map of attainable positive and negative side forces using DFE 1 at various θ locations for 50 deg α and 0 deg β.

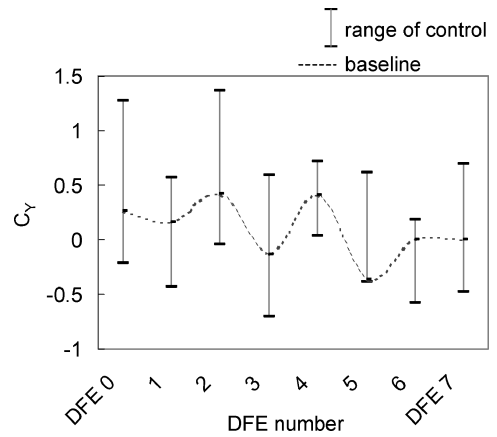

Fig. 14 Control map of side forces generated at 50 deg α and 0 deg β using different DFEs at 22.5 deg θ.

at $\theta = 22.5$ deg. Figure 10 shows the range of forces generated at $\alpha = 40$ deg and $\beta = 0$ deg using DFE configurations as tabulated in Table 3 for cases where DFEs 1–8 were located at $\theta = 22.5$ deg. These tests showed that even though the baseline flow asymmetry tends to behave in a disorderly fashion, the control forces generated by the DFEs were able to successfully cancel and reverse the vortex asymmetry. Figures 11–14 shows similar control maps for $\alpha = 45$ and 50 deg at $\beta = 0$ deg.

Figure 15 shows the time history of yawing-moment coefficient for three different 0 to 60 deg α sweeps (pitch up) at 10 deg/s. The first α sweep was the baseline case where no DFEs were deployed. During the second α sweep, DFE located at $\theta = 22.5$ deg was deployed statically, resulting in a large continuous yawing moment in one direction (positive, yaw right), while similar forces were generated in the opposite direction (negative, yaw left) during the third α sweep where DFE located at $\theta = 157.5$ deg was statically deployed. The DFE circumferential locations of $\theta = 22.5$ and 157.5 deg were chosen because of their ability to create the most significant side forces in opposing directions. A large baseline flow asymmetry in positive yaw direction was observed between $\alpha = 45$ and 60 deg. The DFE at $\theta = 22.5$ deg generated side forces that strengthened the baseline yawing moment in the same direction, whereas the

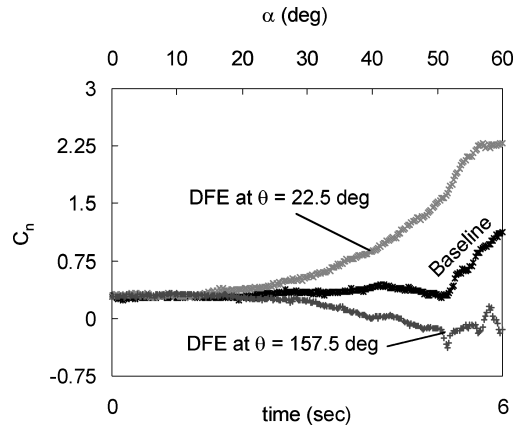

Fig. 15 Time history of yawing-moment coefficient with and without DFEs (baseline) during α sweep from 0–60 deg at pitching rate of 10 deg/s.

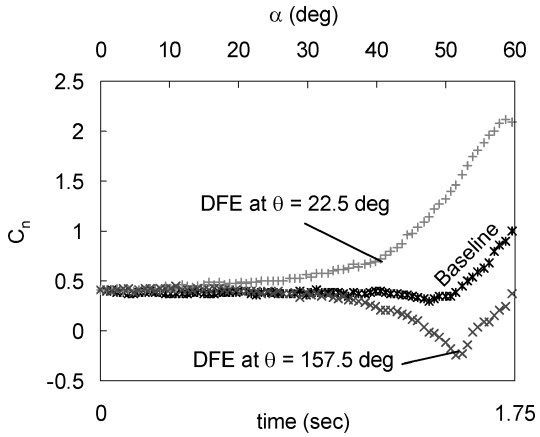

Fig. 16 Time history of yawing-moment coefficient with and without DFEs (baseline) during α sweep from 0–60 deg at pitching rate of 35 deg/s.

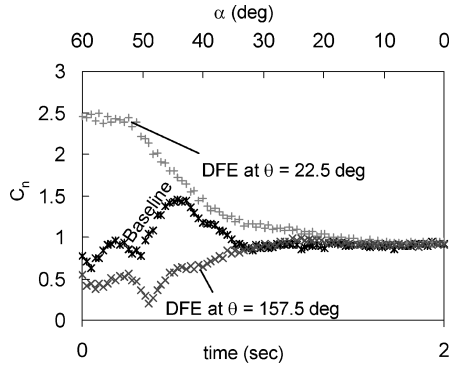

Fig. 17 Time history of yawing-moment coefficient with and without DFEs (baseline) during α sweep from 60–0 deg at pitching rate of 35 deg/s.

DFE at $\theta = 157.5$ deg was able to completely cancel the baseline flow asymmetry and create the opposite yawing moment between $\alpha = 45$ and 60 deg. Similar characteristic curves of α sweeps for pitching rate of 35 deg/s are shown in Fig. 16 (pitch up) and Fig. 17 (pitch down). Comparison of Figs. 16 and 17 demonstrates similar effects of the DFEs and baseline on forebody flow asymmetries.

Control modulation experiments using the closed-loop control system were conducted at $\alpha = 60$ deg and $\beta = 0$ deg. Two DFEs, one located at $\theta = 22.5$ deg and the other at $\theta = 157.5$ deg, similar DFE locations as previous α-sweep tests, were used in these experiments. However, in this case the DFE deployment configuration was actively modified by the controller in real time so as to modulate the generated yawing moments to achieve the commanded (desired) moments. The command input variable C_n, representative of the desired yawing moment (left, right, or zero), was compared to the measured flow state C_n. The error signal was used by the controller to generate mapping functions $f_n(x)$ for both DFEs that contained their deployment configuration (in this case, frequency and duty cycle) for the duration of the controller time step, that is, 80 ms. Based on the updated error signal after 80 ms, new mapping functions with new deployment configuration for both DFEs were generated by the controller. The total PID range for the control modulation experiments varied from -0.5 to 0.5. Individual mapping functions used for the two were $f_1(x) = 1 - (x + 0.5)$ and $f_2(x) = x + 0.5$.

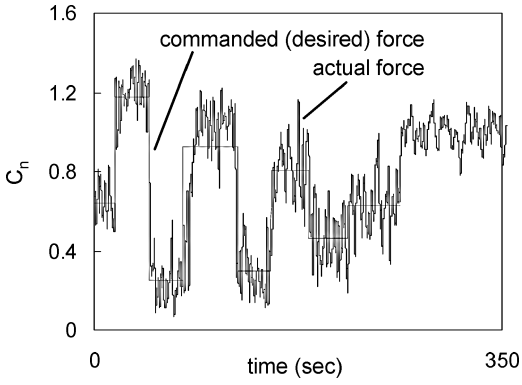

Fig. 18 Time history of actual and commanded yawing-moment coefficient using closed-loop yaw-control system at 60 deg α.

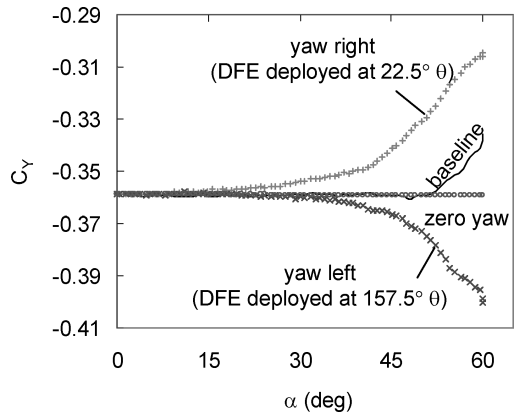

Fig. 19 Control authority of DFEs during α sweep from 0–60 deg at pitching rate of 35 deg/s.

Figure 18 shows a superposition of the commanded signal (desired force) and the actual force as obtained by the closed-loop control system. The user-commanded yaw values ranging from 33 to 100% of the maximum achievable yaw by the DFEs at $\alpha = 60$ deg. The control system was successfully able to generate and maintain desired states (Fig. 18) using two DFEs as activated by the controller system. The dynamically changing input in the form of DFE duty cycles and frequencies led to specific desired patterns of vortex pulses, which were created and convected downstream. The timescale associated with the development of vortical structures by DFEs was dictated by the DFE duty cycle and the forcing frequency and found to be the crucial parameter in achieving the desired level of moment modulation. Figure 19 shows the control maps obtained from different static and closed-loop experiments to demonstrate the ability of the controller to generate negative and positive yawing moments as well as maintain zero-yaw during α sweep from 0 to 60 deg at a pitching rate of 35 deg/s. Figure 20 shows the ability of the closed-loop control system to hold the baseline flow asymmetry to a constant yaw value using DFEs at $\theta = 22.5$ and 157.5 deg and the closed-loop controller.

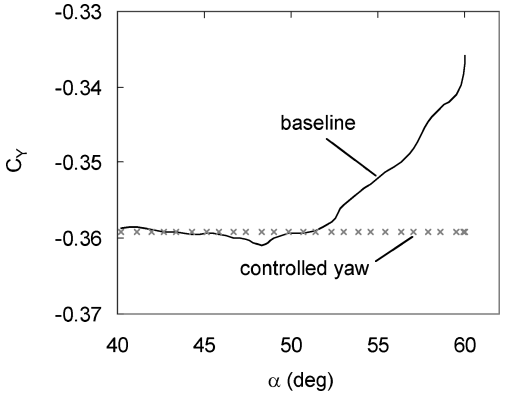

Fig. 20 Controlled yaw using closed-loop control system during α sweep from 0–60 deg at pitching rate of 35 deg/s.

Conclusions

This paper presented an experimental study of a high-alpha yaw-control system for enhanced missile maneuverability and stabilization. It was found that the deployable flow effector configuration parameters—position and frequency of operation—were critical in achieving the desired side forces during both static and dynamic-pitching tests. The control system exploited the time lag associated with the flow response to control inputs to achieve and maintain a desired yawing moment by dynamically changing the actuator duty cycles. The oscillatory control input leads to controlled pulsing dictation of the vortical flowfield around the missile body to sustain a desired vortex state even at natural near bistable conditions. Results demonstrated the ability of the control system to generate and maintain a desired yawing moment (zero, left, and right yaw) using the DFEs, integrated with sensors and a closed-loop controller.

Acknowledgments

This work was supported by the U.S. Air Force Research Laboratory (AFRL) at Wright–Patterson Air Force Base under a Phase II SBIR award. Special thanks go to Michael Valentino of AFRL for granting resources and providing impetus to this research. The authors thank the following individuals for their substantial support of the research program: Troy Prince, Jack DiCocco, Reed Carver, and Frederick Lisy of Orbital Research, Inc.

References

[1]Gapcynski, J. P., "An Experimental Investigation of the Flow Phenomena over Bodies at High Angles of Attack at a Mach Number of 2.0," NACA RM-L55H29, Oct. 1955.

[2]Gowen, F. E., and Perkins, E. W., "A Study of the Effect of Body Shape of the Vortex Wakes of Inclined Bodies at a Mach Number of 2," NACA RM-A53117, Dec. 1958.

[3]Ericsson, L. E., and Reding, J. P., "Asymmetric Flow Separation and Vortex Shedding on Bodies of Revolution," *Tactical Missile Aerodynamics*, edited by M. J. Hemsch, Vol. 141, Progress in Aerospace and Aeronautics, AIAA, Washington, DC, 1991, pp. 391–452.

[4]Thomson, K. D., and Morrison, D. F., "On the Asymmetric Vortex Shedding from Slender Cylindrical Bodies at Large Angles of Yaw," Weapon Research Establishment, TN-HSA 106, Australia, May 1965.

[5]Ericsson, L. E., "Unsteady Flow Separation on Slender Bodies at High Angles of Attack," AIAA Paper 90-2835, Jan. 1990.

[6]Pick, G. S., "Investigation of Side Forces on Ogive-Cylinder Bodies at High Angles of Attack in the $M = 0.5$ to 1.1 Range," AIAA Paper 71-570, June 1971.

[7]Ashley, H., "On the Feasibility of Low-Speed Aircraft Maneuvers Involving Extreme Angles of Attack," *Journal of Fluids and Structures*, Vol. 1, July 1987, pp. 319–335.

[8]Wardlaw, A. B., Jr., "High Angle of Attack Missile Aerodynamics," LS-98, AGARD, March 1978 (Paper 5).

[9]Jorgenson, L. H., "Prediction of Aerodynamic Characteristics of Slender Bodies Alone and with Lifting Surfaces to High Angles of Attack," CP-247, AGARD, Oct. 1978 (Paper 28).

[10]Chapman, G. T., and Keener, E. R., "The Aerodynamics of Bodies of Revolution at Angles of Attack to 90°," AIAA Paper 79-0023, Jan. 1979.

[11]Ericsson, L. E., and Reding, J. P., "Review of Vortex-Induced Asymmetric Loads—Part I," *Zeitschrift fuer Flugwissenschaften und Weltraumforschung*, Vol. 5, No. 3, 1981, pp. 162–174.

[12]Ericsson, L. E., and Reding, J. P., "Review of Vortex-Induced Asymmetric Loads—Part II," *Zeitschrift fuer Flugwissenschaften und Weltraumforschung*, Vol. 5, No. 6, 1981, pp. 349–366.

[13]Herbst, W. B., "Supermaneuverability," *Proceedings of the Workshop on Unsteady Separated Flow*, edited by M. S. Francis and M. W. Luttges, U.S. Air Force Academy, Colorado Spring, CO, 1983, pp. 1–9.

[14]Ericsson, L. E., and Beyers, M. E., "Conceptual Fluid/Motion Coupling in the Herbst Supermaneuver," *Journal of Aircraft*, Vol. 34, No. 3, 1997, pp. 271–277.

[15]Rao, D. M., "Side Force Alleviation on Slender, Pointed Forebodies at High Angles of Attack," *Journal of Aircraft*, Vol. 16, No. 11, 1979, pp. 763–768.

[16]Modi, V. J., and Stewart, A. C., "Approach to Side Force Alleviation Through Modification of the Pointed Foreody Geometry," AIAA Paper 90-2834, Jan. 1990.

[17]Fisher, D. F., and Cobleigh, B. R., "Controlling Forebody Asymmetries in Flight-Experience with Boundary Layer Transition Strips," NASA TM 4595, July 1994.

[18]Ericsson, L. E., "Unsteady Flow Separation on Slender Bodies at High Angles of Attack," AIAA Paper 90-2835, Jan. 1990.

[19]Maynes, R. D., and Gebert, G. A., "Rotating Nose Tip Effects on Slender Body Aerodynamics at High Angles of Attack," *Journal of Spacecraft and Rockets*, Vol. 32, No. 6, 1995, pp. 944–950.

[20]Stahl, W., "Suppression of Asymmetry of the Vortex Flow Behind a Circular Cone at High Incidence," AIAA Paper 89-3372-CP, Aug. 1989.

[21]Ng, T. T., "Effect of a Single Strake on the Forebody Vortex Asymmetry," *Journal of Aircraft*, Vol. 27, No. 9, 1990, pp. 161–184.

[22]Sharic, D., Portnoy, H., and Rom, J., "A Study of the Effects of Jets Injected from a Slender Body of Revolution on the Side Forces Acting on it at Large Angles of Attack in Low Speeds," Dept. of Aeronautical Engineering, Technion—Israel Inst. of Technology, TAE 337, Haifa, Israel, 1978.

[23]Roos, F. W., "Microblowing for High-Angle-of-Attack Flow Control on a Fighter Aircraft," AIAA Paper 96-0543, Jan. 1996.

[24]Malcolm, G. N., and Ng, T. T., "Aerodynamic Control of Fighter Aircraft by Manipulation of Forebody Vortices," CP-497, AGARD, Nov. 1991 (Paper 15).

[25]Williams, D., and Bernhardt, J., "Proportional Control of Asymmetric Forebody Vortices with the Unsteady Bleed Technique," AIAA Paper 90-1629, June 1990.

[26]Bernhardt, J., and Williams, D., "Effect of Reynolds Number on Control of Forebody Asymmetry by Suction and Bleed," AIAA Paper 93-3265, July 1993.

[27]Patel, M. P., Ng, T. T., Lisy, F. J., Prince, T. S., and DiCocco, J. M., "MEMS Deployable Flow Effectors for Missile Control," 20th AIAA Missile Sciences Conf., 2000.

[28]Buffington, J. M., and Adams, R. J., "Nonlinear Vortex Flow Control for High Angle of Attack Maneuvering," *Control Engineering Practice*, Vol. 3, No. 5, 1995, pp. 631–642.

[29]Bernhardt, J. E., and Williams, D. R., "Closed-Loop Control of Forebody Flow Asymmetry," *Journal of Aircraft*, Vol. 37, No. 3, 2000, pp. 491–498.

[30]Brandon, J. M., Simon, J. M., Owens, B. D., and Kiddy, J. S., "Free-Flight Investigation of Foreody Blowing For Stability and Control," AIAA Paper 96-3444, July 1996.

[31]Malcolm, G. N., "Forebody Vortex Control—A Progress Review," AIAA Paper 93-3540, Aug. 1993.

[32]Jacob, Kay, "Forebody Aerodynamic Asymmetry on a Full-Scale F-15 Radome," AIAA Paper 2000-4104, Aug. 2000.

M. S. Miller
Associate Editor